JCI The Journal of Clinical Investigation

Human ovarian carcinoma–associated mesenchymal stem cells regulate cancer stem cells and tumorigenesis via altered BMP production

Karen McLean, … , Kathleen R. Cho, Ronald J. Buckanovich

J Clin Invest. 2011;121(8):3206-3219. https://doi.org/10.1172/JCI45273.

Research Article **Oncology**

Accumulating evidence suggests that mesenchymal stem cells (MSCs) are recruited to the tumor microenvironment; however, controversy exists regarding their role in solid tumors. In this study, we identified and confirmed the presence of carcinoma-associated MSCs (CA-MSCs) in the majority of human ovarian tumor samples that we analyzed. These CA-MSCs had a normal morphologic appearance, a normal karyotype, and were nontumorigenic. CA-MSCs were multipotent with capacity for differentiating into adipose, cartilage, and bone. When combined with tumor cells in vivo, CA-MSCs promoted tumor growth more effectively than did control MSCs. In vitro and in vivo studies suggested that CA-MSCs promoted tumor growth by increasing the number of cancer stem cells. Although CA-MSCs expressed traditional MSCs markers, they had an expression profile distinct from that of MSCs from healthy individuals, including increased expression of BMP2, BMP4, and BMP6. Importantly, BMP2 treatment in vitro mimicked the effects of CA-MSCs on cancer stem cells, while inhibiting BMP signaling in vitro and in vivo partly abrogated MSC-promoted tumor growth. Taken together, our data suggest that MSCs in the ovarian tumor microenvironment have an expression profile that promotes tumorigenesis and that BMP inhibition may be an effective therapeutic approach for ovarian cancer.

Human ovarian carcinoma–associated mesenchymal stem cells regulate cancer stem cells and tumorigenesis via altered BMP production

Karen McLean,[1] Yusong Gong,[2] Yunjung Choi,[2] Ning Deng,[2] Kun Yang,[2] Shoumei Bai,[2] Lourdes Cabrera,[1] Evan Keller,[3,4] Laurie McCauley,[3] Kathleen R. Cho,[3] and Ronald J. Buckanovich[1,2]

[1]Division of Gynecologic Oncology, Department of Obstetrics and Gynecology, [2]Division of Hematology Oncology, Department of Internal Medicine, [3]Department of Pathology, and [4]Department of Urology, University of Michigan Medical Center, Ann Arbor, Michigan, USA.

Accumulating evidence suggests that mesenchymal stem cells (MSCs) are recruited to the tumor microenvironment; however, controversy exists regarding their role in solid tumors. In this study, we identified and confirmed the presence of carcinoma-associated MSCs (CA-MSCs) in the majority of human ovarian tumor samples that we analyzed. These CA-MSCs had a normal morphologic appearance, a normal karyotype, and were nontumorigenic. CA-MSCs were multipotent with capacity for differentiating into adipose, cartilage, and bone. When combined with tumor cells in vivo, CA-MSCs promoted tumor growth more effectively than did control MSCs. In vitro and in vivo studies suggested that CA-MSCs promoted tumor growth by increasing the number of cancer stem cells. Although CA-MSCs expressed traditional MSCs markers, they had an expression profile distinct from that of MSCs from healthy individuals, including increased expression of BMP2, BMP4, and BMP6. Importantly, BMP2 treatment in vitro mimicked the effects of CA-MSCs on cancer stem cells, while inhibiting BMP signaling in vitro and in vivo partly abrogated MSC-promoted tumor growth. Taken together, our data suggest that MSCs in the ovarian tumor microenvironment have an expression profile that promotes tumorigenesis and that BMP inhibition may be an effective therapeutic approach for ovarian cancer.

Introduction

There is strong evidence that mesenchymal stem cells (MSCs) are recruited to the tumor microenvironment. Based on this tropism of MSCs for the tumor microenvironment, numerous studies have suggested that MSCs could potentially be used as therapeutic vectors to target the tumor (1). Before such an approach is feasible in humans, it is essential to understand the function of MSCs in the tumor microenvironment. To date, the function of MSCs in cancer remains controversial.

Several studies have suggested that MSCs restrict cancer growth. MSCs suppressed growth of MCF-7 breast cancer cells through dickkopf-1–mediated (Dkk-1–mediated) inhibition of the Wnt signaling pathway (2). Similarly Dkk-1 was implicated in the suppression of leukemia cell growth (3). Finally, hepatoma cell growth was significantly inhibited by MSC-conditioned media; MSC-conditioned media induced apoptosis and decreased the expression of Bcl-2, c-Myc, β-catenin, and survivin (4).

Contrary to these observations, other studies have suggested that MSCs promote tumorigenesis. One study reported that MSCs promoted tumor cell viability and proliferation and reduced apoptotic cell death in multiple cell types (5). MSCs have also been reported to promote the proliferation of melanoma cells (6). More recently, human MSCs were shown to enhance the growth and metastatic capacity of breast cancer cells (7, 8). Breast cancer cells were shown to stimulate MSC production of the chemokine CCL5, which then stimulated breast cancer cell motility and invasion (7). Growth enhancement has been reported to be specifically through the interaction of MSCs and breast cancer stem cells (CSCs) (9). Finally, in an ovarian cancer model, normal human bone marrow–derived MSCs were shown to ultimately lead to an enhancement of tumor growth via MSC differentiation into tumor-associated fibroblasts, which produced numerous growth factors to support angiogenesis and tumor cell growth (10).

Importantly, the above studies were performed with either MSC lines or healthy donor-derived MSCs. Little is known about MSCs or tumor-associated MSCs in cancer patients. Study of tumor-associated MSCs is important, as host cells within the tumor microenvironment often have an altered phenotype, which can contribute to tumorigenesis (11–14). Several groups have analyzed MSCs in the bone marrow of patients with hematologic malignancies and suggest that cancer-associated MSCs may be abnormal. While bone marrow MSCs (BM-MSCs) in patients with multiple myeloma appeared phenotypically and karyotypically normal, they had reduced capacity to inhibit T cell proliferation and produced abnormally high levels of IL-6, suggesting functional impairment (15). Similarly, BM-MSCs in leukemia patients do not carry chromosomal abnormalities commonly associated with leukemic transformation (16, 17) but may function abnormally, with limited proliferation capacity, impaired differentiation, and a decreased ability to support hematopoiesis (17). Myeloma-associated MSCs have been reported to have a distinct genomic profile as compared with that of cells from normal donors (18).

Authorship note: Karen McLean and Yusong Gong contributed equally to this work.
Conflict of interest: The authors have declared that no conflict of interest exists.
Citation for this article: *J Clin Invest.* 2011;121(8):3206–3219. doi:10.1172/JCI45273.

Less is known about MSCs in human solid tumors. MSCs have been identified in bone sarcomas, lipomas, and infantile hemangiomas (19–21). It has been proposed that MSCs may in fact be the source of the mesenchymal malignancies in these studies; thus, it is difficult to say whether these data would apply to MSCs in epithelial cancers, such as ovarian carcinoma (22, 23). A recent study in lung cancer patients suggested that $CD105^+$ mesenchymal progenitor cells were present in pulmonary arterial blood in greater than 90% of lung cancer patients (24). Interestingly, MSCs were also recently reported as present in 13 out of 20 human gastric cancer tissues (25). These cells appeared phenotypically identical to healthy donor cells. Gastric cancer-associated MSCs and healthy donor MSCs had a similar gene expression pattern based upon flow cytometry, immunohistochemistry, and/or RT-PCR analysis of 23 different genes. Gastric cancer-associated MSCs also showed normal differentiation capacity. The functional role of these MSCs on cancer growth was not tested.

We report here the identification, purification, and in-depth phenotypical and functional characterization of human ovarian carcinoma-associated MSCs (CA-MSCs). We find that MSCs can be identified in greater than 90% of primary human ovarian carcinomas. These MSCs are nontumorigenic, have a normal karyotype, express the anticipated cell surface markers, and demonstrate an increased capacity for multipotent differentiation. Functionally, human ovarian CA-MSCs, when compared with healthy donor MSCs, were more effective at promoting tumor growth in vivo. Similarly, CA-MSCs promoted tumor sphere growth in vitro associated with an increase in tumor "stemness." Expression analysis of CA-MSCs demonstrated that they have a unique gene expression profile to our knowledge, including altered expression levels of BMP pathway proteins. BMP2 treatment of ovarian cancer cell lines and primary ovarian tumor cells was found to significantly increase the percentage of CSCs. In vitro and in vivo inhibition of BMP signaling with Noggin inhibited the ability of CA-MSCs to promote tumor stemness and tumor growth. Thus, ovarian cancer MSCs appear to promote tumorigenesis, at least in part, through altered BMP signaling.

Results

Isolation of ovarian cancer–associated MSCs. In the process of characterizing host cells in the ovarian cancer microenvironment, we identified a cellular population with the morphology of CFU-fibroblastic (CFU-F) (Figure 1A), the sine qua non of MSCs (26). FACS analysis of human ovarian tumor ascites demonstrated that cells with the surface protein expression pattern of MSCs ($CD44^+$, $CD73^+$, $CD90^+$) were relatively abundant (~6% of cells; range, 1%–11%; Figure 1B). Percentages in solid tumors were lower (~0.3%; data not shown), although this may relate to the inability to release cells in the tumor stroma using mechanical dissection. Attempts to isolate these cells using FACS or magnetic bead isolation led to poor viability or were hampered by contamination with tumor cells. We therefore developed isolation and culture conditions favoring the growth of MSCs. We found that placing washed fresh tumor slices on plastic culture dishes in Mammary Epithelial Basal Medium (MEBM) with supplements resulted in the formation of relatively pure CFU-F colonies (Figure 1A). These colonies could then be expanded and replated at limiting dilutions to generate pure ovarian CA-MSC clones.

Several assays were performed with at least 6 CA-MSC specimens to confirm these clones were not contaminated with other highly proliferative cells, mainly cancer cells and endothelial cells. First, these clones were returned to mesenchymal media, RPMI 10, DMEM, or EBM2 media. No endothelial or epithelial colonies developed (data not shown). Furthermore, we tested the tumorigenicity of these cells as compared with that of primary tumor cells from patients. 1×10^6 CFU-F cells from 7 separate patients were incapable of forming tumors. In contrast, 1×10^5 primary tumor cells from 4 out of 7 matched patient samples were capable of forming subcutaneous tumors (data not shown). Additionally, we have karyotyped MSCs isolated from 2 different patients, and both samples revealed normal 46, XX karyotype (data not shown and Supplemental Figure 1A; supplemental material available online with this article; doi:10.1172/JCI45273DS1), supporting the hypothesis that these cell populations are not derived from tumor cells, which have many karyotype abnormalities.

We next performed qRT-PCR for both endothelial and tumor-specific markers. Limiting dilution assays demonstrated that this assay can detect 1 contaminating cell in approximately 10,000 (data not shown). As controls, we used adipose MSCs, BM-MSCs, and an MSC clone isolated from normal ovary in a manner analogous to the derivation of the CA-MSCs. CA-MSC lines had no expression of the endothelial markers VE-Cadherin, CD31, and ENOS (Figure 1C). Similarly, we did not see the expression of multiple tumor cell markers, including MUC1, MUC16, HE4, EpCAM, or cytokeratin 20 (CK20; Figure 1C). We did observe the expression of cytokeratin 7 (CK7) in 2 out of 8 of CA-MSCs (Figure 1C and data not shown). The expression of CK7 in these samples was higher than that of whole tumor, suggesting that this was not trace cellular contamination. MSCs derived from normal ovary also expressed modest levels of CK7. CK7 expression appears related to culture in epithelial media; CK7 expression was decreased when MSCs were cultured in mesenchymal media (Supplemental Figure 1B), suggesting CK7 expression in these lines could be related to a mesenchymal-to-epithelial transition. However, in order to assure integrity of our results, CA-MSC lines with significant expression of CK7 were excluded from further analysis.

CA-MSC surface expression and differentiation capacity. We next confirmed the mesenchymal phenotype of CA-MSCs based upon both surface marker expression and functional differentiation capacity. Flow cytometry of CA-MSCs confirmed a phenotype consistent with the published cell surface molecule expression profile for MSCs (27). CA-MSCs, like all control MSCs, lacked expression of leukocyte, hematopoietic stem cell, and endothelial progenitor cell markers, including CD14, CD45, CD34, and CD133, but expressed CD105 (SH2), CD73 (SH3), CD90 (Thy-1), and CD44 (Supplemental Figure 1C and data not shown). Interestingly, MEBM ovarian CA-MSCs expressed reduced levels of CD90 and CD105, relative to those of controls (Supplemental Figure 1D and data not shown), suggesting that CA-MSCs may have an altered phenotype.

The true phenotypic hallmark of MSCs is multipotent differentiation capacity; MSCs are capable of differentiating into multiple tissue types, including bone, cartilage, and adipose (26). We therefore tested the ability of the ovarian CA-MSCs to differentiate into these various tissue lineages in vitro when grown in appropriate culture conditions. All 6 assayed ovarian cancer MSCs demonstrated successful differentiation into these 3 tissue types (Figure 1D). Primary epithelial ovarian carcinoma cell lines tested demonstrated poor viability under differentiation culture conditions, and no positive clones were observed (data not shown).

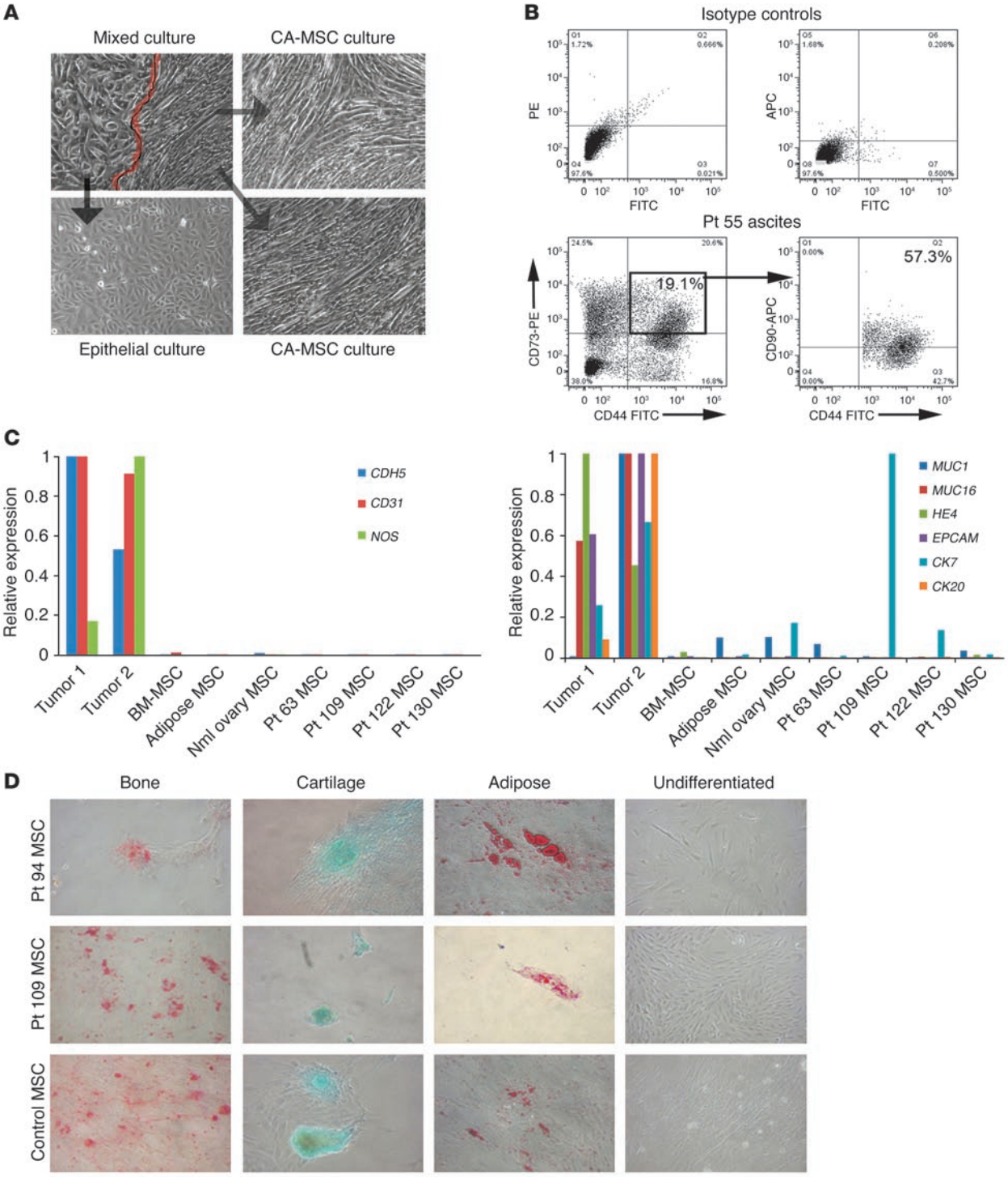

Figure 1

Isolation of ovarian CA-MSCs. (**A**) Photograph of mixed primary ovarian tumor culture (top left) and the resultant, distinct purified colonies of epithelial tumors cells or CA-MSCs. Original magnification, ×100. (**B**) FACS analysis of primary ovarian tumor ascites, demonstrating $CD44^+CD73^+CD90^+$ cells. (**C**) qRT-PCR to confirm CA-MSC purity. CA-MSC lines have no significant expression of the indicated endothelial or epithelial cell markers. Whole primary tumor mRNA (tumor) was used as a positive control. Expression levels were relative to the sample with maximal expression defined as 1. Nml, normal. (**D**) CA-MSCs demonstrate multipotent differentiation capacity in differential culture conditions. Specific cell stains used were Alizarin Red-S for bone, alcian blue for cartilage, and Oil Red O for adipose. Original magnification, ×100. Pt, patient.

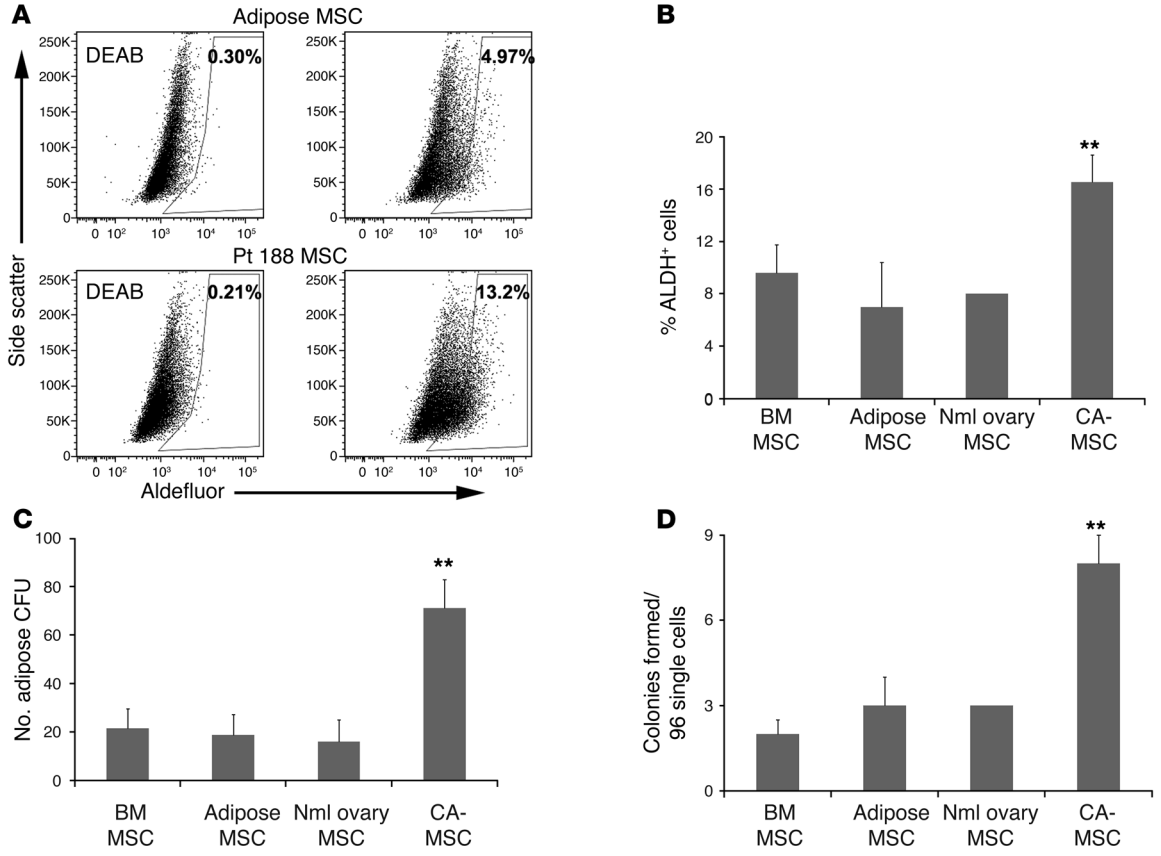

Figure 2

CA-MSCs demonstrate increased stem cell capacity. (**A**) FACS analysis demonstrating that CA-MSCs have an increased percentage of Aldefluor$^+$ cells compared with adipose MSC controls. Numbers represent the percentage of Aldefluor$^+$ cells. (**B**) Average percentage of ALDH$^+$ cells in indicated control cells and CA-MSCs. (**C**) Adipose CFUs formed per 50,000 cells in the indicated control cells and CA-MSCs. (**D**) Single cell clones generated from the indicated control cells and CA-MSCs. (**A**–**D**) BM-MSCs, $n = 2$; adipose MSCs, $n = 3$; normal ovary MSCs, $n = 1$; CA-MSCs, $n = 5$. $^{**}P < 0.05$. Error bars represent standard deviations.

A recent publication suggests that the multipotent stem cells within MSC cultures can be identified by the presence of aldehyde dehydrogenase enzymatic activity (ALDH) (9). We therefore next assayed ALDH activity in CA-MSCs and controls to compare the stem cell phenotype. We observed a 2-fold increase in the percentage of ALDH$^+$ cells in CA-MSCs as compared with that in control MSCs, including healthy donor adipose-derived MSCs, BM-MSCs, and normal ovary-derived MSCs (Figure 2, A and B). Using the adipogenesis assay, we next assayed the efficiency of differentiation of CA-MSCs versus that of control MSCs. Consistent with the increased ALDH expression, we observed an approximate 3.5-fold increase in the adipogenic capacity of CA-MSCs versus that of controls (Figure 2C). Finally, we generated single cell clones from a CA-MSC and a control MSC. The CA-MSC demonstrated a 2.5-fold increased capacity to generate single cells clones versus that of controls (Figure 2D).

CA-MSCs therefore have the morphologic, surface marker expression, and functional phenotype of adipose and bone marrow–derived MSCs. These data strongly suggest that we have successfully isolated MSCs from ovarian cancer tissue. Interestingly, our findings suggest that CA-MSCs may have properties such as increased stemness that distinguish them from healthy tissue MSCs.

The impact of ovarian CA-MSCs on tumor growth in murine models of cancer. MSCs have been reported to either promote or suppress cancer growth, depending on the tumor type and the experimental conditions (2, 4, 5, 8, 10, 28–30). We next sought to analyze the impact of ovarian CA-MSCs on ovarian tumor growth, including the relative impact as compared with that of healthy donor MSCs. We assessed the growth of 1×10^6 SKOV3 cells injected subcutaneously into the axillae of immune-compromised mice alone ($n = 25$) or of 5×10^5 SKOV3 cells combined with either 5×10^5 control MSCs ($n = 10$ adipose MSCs and $n = 5$ BM-MSCs) or 5×10^5 SKOV3 CA-MSCs ($n = 20$) in 2 independent experiments. We observed that BM-MSCs did not significantly increase tumor growth; however, adipose-derived MSCs significantly enhanced the growth of SKOV3 tumors (Figure 3A and Supplemental Figure 2A). Interestingly, when CA-MSCs were grown together with SKOV3 cells, we observed a greater enhancement of ovarian cancer cell growth as compared with that with SKOV3 cells grown with adipose MSCs (Figure 3A). Similar results were obtained with ovarian cancer MSCs derived from 6 different patients with 5–10 mice per patient-derived ovarian cancer MSC cell line (Supplemental Figure 2A and data not shown). In addition, similar results were also observed when MSCs were grown with the ovarian cancer cell lines Hey1 and Ovcar8 (data not shown).

In order to confirm that these results were secondary to increased tumor cell number and not expansion of the MSCs, we repeated these experiments using luciferase-labeled SKOV3 cells. SKOV3^{luc}

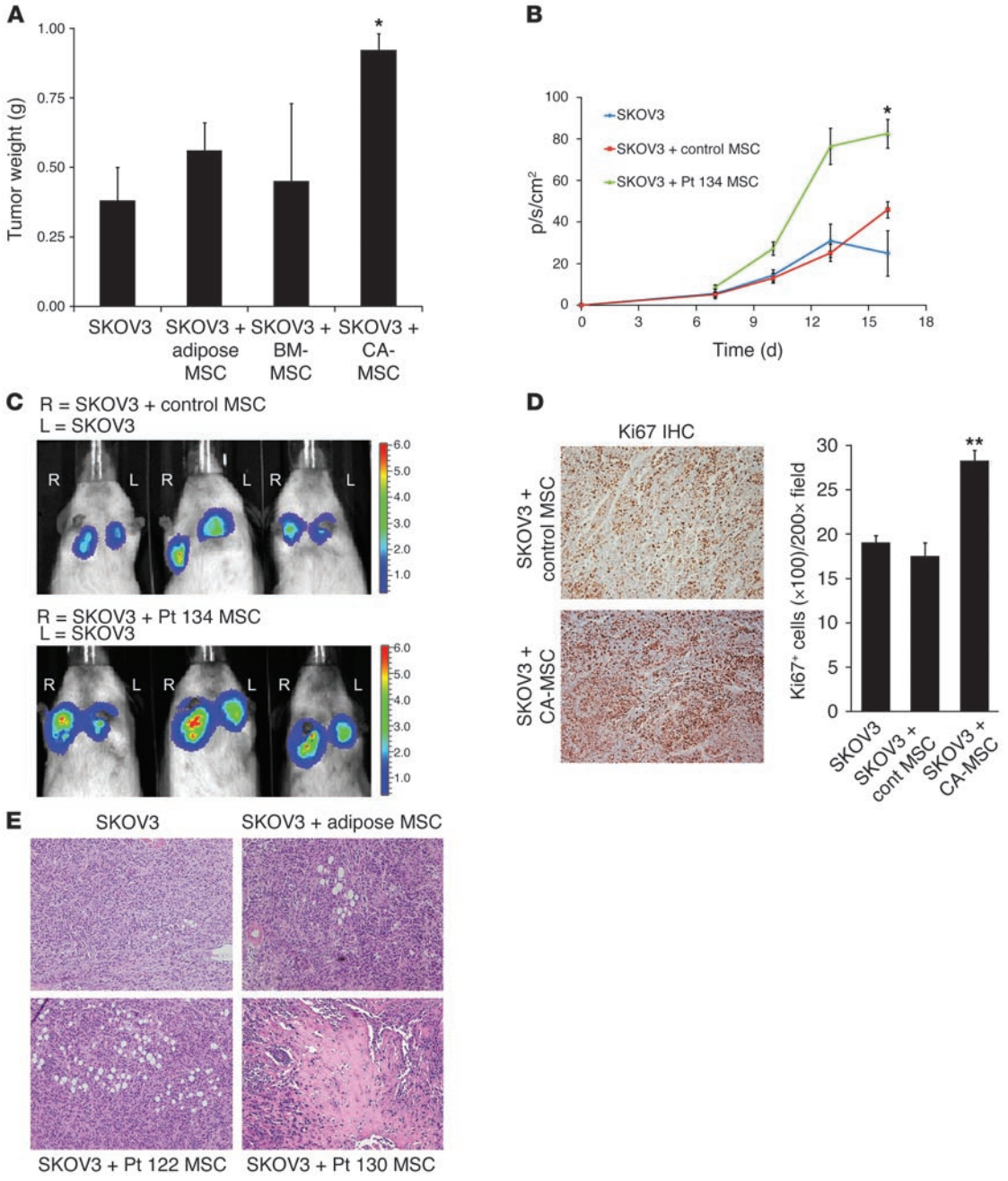

Figure 3

CA-MSCs promote ovarian tumorigenesis more than control MSCs. (**A**) Tumor weights of SKOV3 tumors grown alone or with the indicated MSCs (SKOV3 plus control MSCs, $n = 10$; SKOV3 plus CA-MSCs, $n = 20$; pooled results, $n = 5$ for 4 CA-MSC cell lines). Results are representative of 2 independent experiments. (**B** and **C**) Bioluminescent-based tumor growth curve of SKOV3-luciferase tumors alone or in combination with the indicated MSCs (control MSCs, $n = 10$ and Pt 134 MSCs, $n = 8$, in 2 independent experiments). Signal intensity mapping for tumors is shown (p/s/cm^2). (**D**) Ki67 immunohistochemistry and quantification from SKOV3$^+$adipose MSC and SKOV3$^+$CA-MSC tumors. Original magnification, ×100. Cont, control. (**E**) Hematoxylin and eosin stains of paraffin-embedded tumor specimens grown with MSCs or CA-MSCs, demonstrating tumor adipocytes (top right and bottom left). Tumors with CA-MSCs demonstrated areas of early bone formation (bottom right). Original magnification, ×40. All results represent means with standard deviations. $^*P < 0.01$; $^{**}P < 0.001$.

plus CA-MSC tumors demonstrated a consistent increase in luciferase activity as compared with that of control SKOV3^{luc} tumors and SKOV3^{luc} plus adipose MSC tumors (Figure 3, B and C), thus confirming that CA-MSCs increase SKOV3 tumor cell number. Furthermore, changing the absolute number of MSCs injected (1.5×10^5, 5×10^5, or 1.5×10^6 MSCs) had a modest dose effect but no significant impact on tumor size (Supplemental Figure 2C).

Histological analysis of these tumors was performed to determine a potential mechanism for the increased tumorigenesis of tumors grown with CA-MSCs compared with that of controls. Consistent

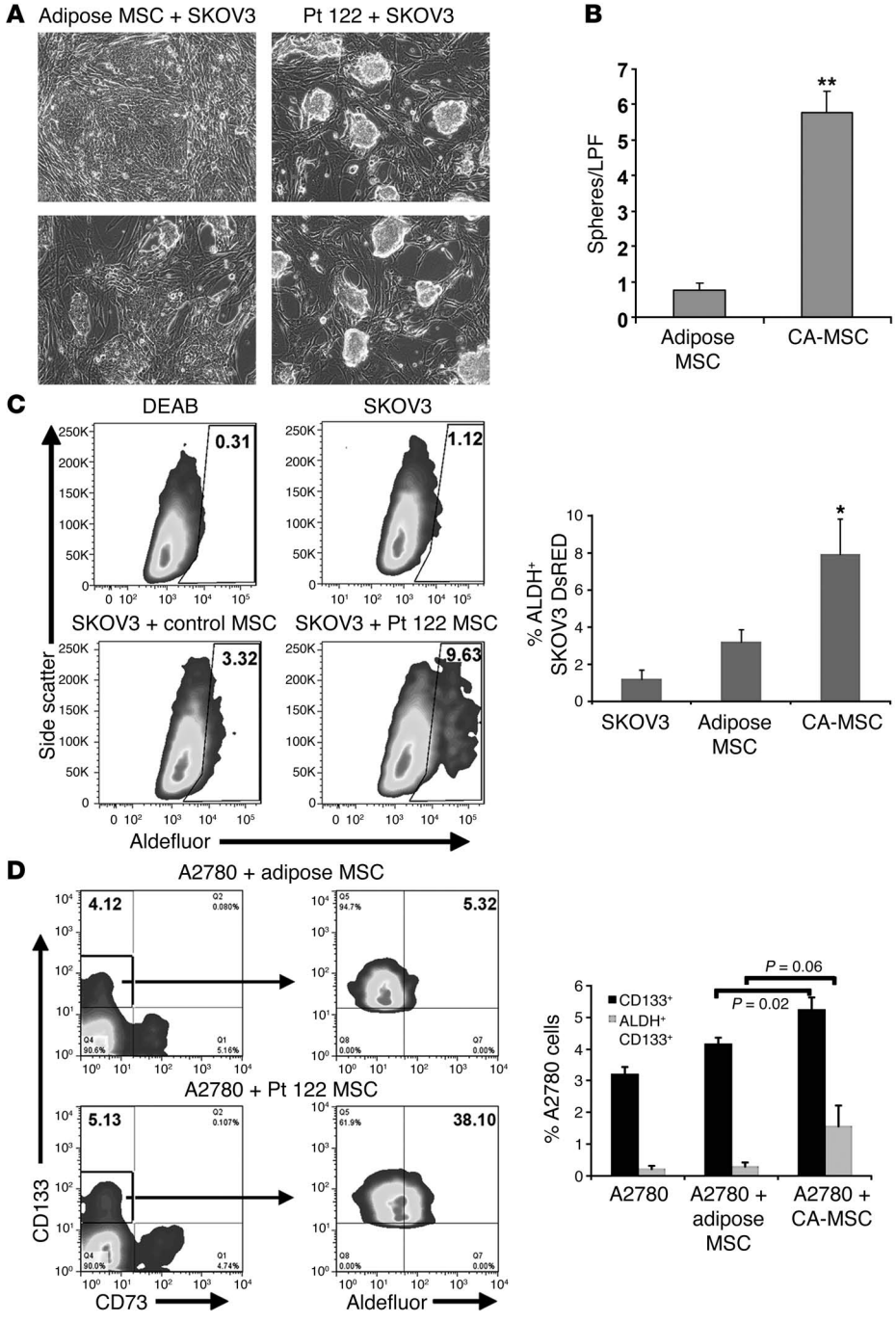

Figure 4

CA-MSCs increase the number of CSCs. (**A**) SKOV3 cells, cocultured with either adipose MSCs or CA-MSCs, demonstrating sphere formation in the presence of CA-MSCs. Original magnification, ×100. (**B**) Average number of spheres per low-powered field (LPF) in SKOV3 cells with control versus CA-MSCs. $^{**}P < 0.001$. (**C**) Representative Aldefluor analysis of DsRED SKOV3 cells either alone or cocultured with Adipose MSCs or CA-MSCs and averages from 3 independent experiments. DEAB was used as a negative control. Numbers represent the percentage of Aldefluor$^+$ cells. $^*P < 0.01$. (**D**) Representative FACS analysis demonstrating the percentage of CD133$^+$CD73$^-$ ALDH$^+$ A2780 cells cocultured with adipose MSCs or CA-MSCs and the average percentage of ALDH$^+$ cells or ALDH$^+$CD133$^+$ A2780 cells. Numbers in the top left quadrant represent the number of CD133$^+$/CD73$^-$ cells; numbers in the top right quadrant represent the number of CD133$^+$/Aldefluor$^+$ cells. Error bars represent standard deviations.

with increased tumor cell growth, there was a statistically significant 36% increase in Ki67 staining in CA-MSC tumors versus that of controls (Figure 3D). Tunnel staining demonstrated no clear differences in apoptosis between CA-MSCs and control groups (data not shown). Immunohistochemical analysis of vascular CD31 expression demonstrated that there was a slight increased microvascular density between tumors with and without MSCs. However, we observed no difference in vascular density between the tumors with control MSCs and CA-MSCs (Supplemental Figure 3A and data not shown), suggesting that increased angiogenesis is not the primary cause of CA-MSC–mediated tumor growth. Additionally, we did not detect significant differences in the amount of fibroblastic/stromal tissue present in tumors generated with control MSCs versus CA-MSCs (Figure 3E). We observed increased adipose tissue in tumors with CA-MSCs from some patient samples, compared with that of control MSCs (Figure 3E). These were confirmed to be adipocytes using Oil Red O stain (Supplemental Figure 3B). We also observed areas of tumor that had the appearance of early bone formation (Figure 3E). A Masson's trichrome stain suggested that these were regions of precalcified bone (Supplemental Figure 3B). For several human genes involved in adipose and bone differentiation, mRNA expression levels were clearly elevated in tumors with

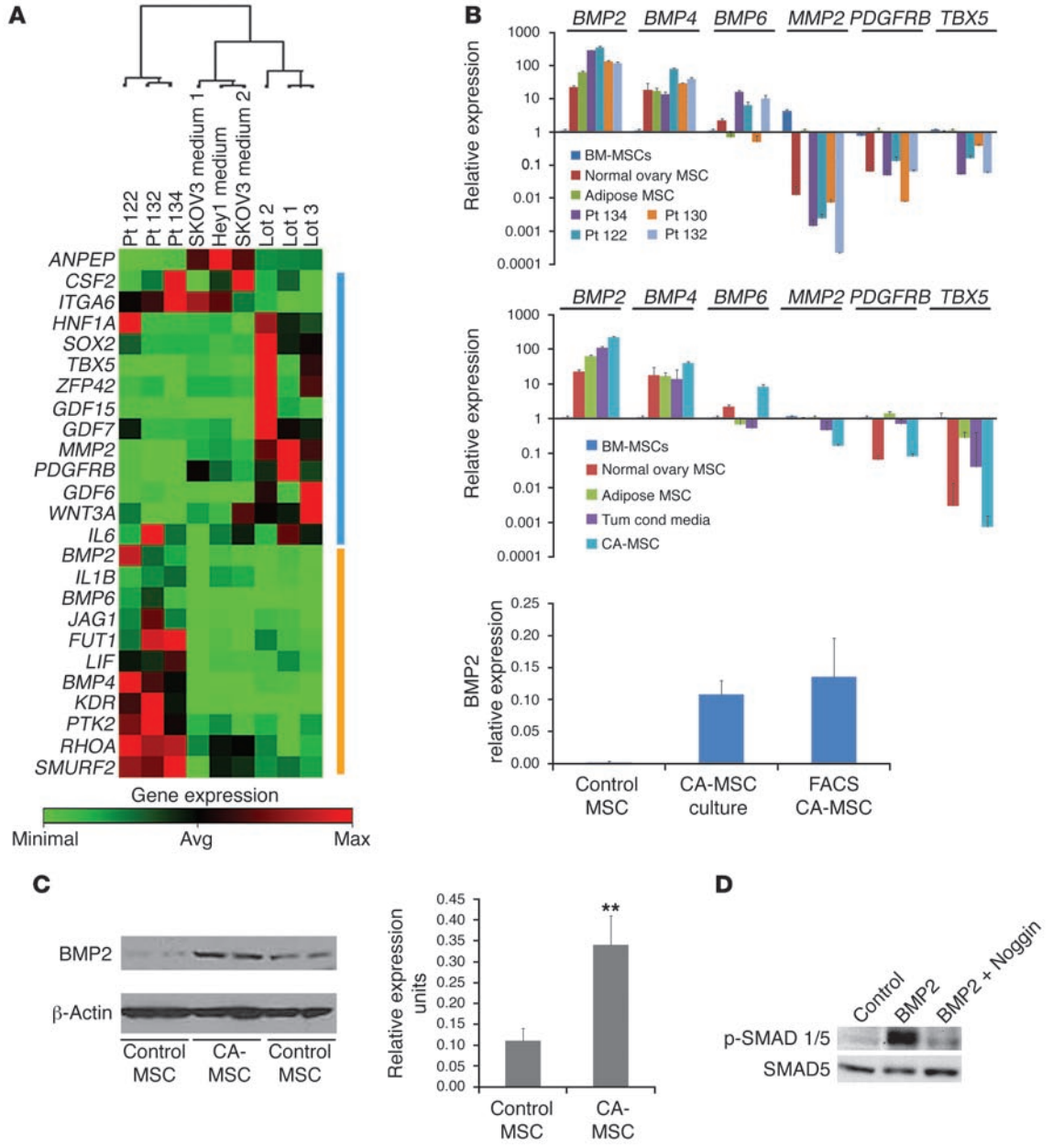

Figure 5

CA-MSCs have a gene expression profile distinct from that of control MSCs. (**A**) Heat map of gene expression of MSC-associated gene expression in CA-MSCs, adipose control MSCs (lot 1, 2, 3), and control MSCs cultured with tumor-conditioned media from either SKOV3 or Hey1 ovarian tumor cells. The blue line indicates genes differentially expressed in CA-MSCs and MSCs treated with tumor-conditioned media. The orange bar indicates genes that appear to be uniquely expressed in CA-MSCs. Avg, average; max, maximum. (**B**) qRT-PCR using independently derived gene-specific primers performed to confirm differential expression of the indicated genes in control versus 4 CA-MSC–derived cell isolates (top), pooled analysis of qRT-PCR results (middle), and BMP2 expression in controls, cultured CA-MSCs, and FACS-isolated CA-MSCs (bottom). Tum cond media, tumor-conditioned media. (**C**) Western blot demonstrating increased BMP2 protein expression in adipose control MSCs and CA-MSCs. Quantification of BMP2 band intensity from immunoblotting is shown with average and standard deviation indicated. $^{**}P = 0.03$. (**D**) Western blot detection of p-SMAD 1/5 before and after treatment with BMP2 in the presence or absence of the BMP inhibitor Noggin.

MSCs, suggesting these adipose/pre-bone tissues were human in origin (Supplemental Figure 3C). The generation of adipose and bone deposition was consistent with the multipotent capacity of CA-MSCs. Taken together, these data suggest that ovarian CA-MSCs promote tumor growth and that increased tumor size is primarily due to the increased proliferation of epithelial tumors cells.

The impact of MSCs on ovarian CSCs. In order to assess the impact of MSCs on tumor cells, we cocultured control MSCs or CA-MSCs with ovarian tumor cell lines in vitro. Interestingly, while tumor cells cocultured with control MSCs mostly grew adherent to the plate, tumor cells cultured in the presence of CA-MSCs grew in suspension in large spheroids (Figure 4A). The ability to grow in suspension in

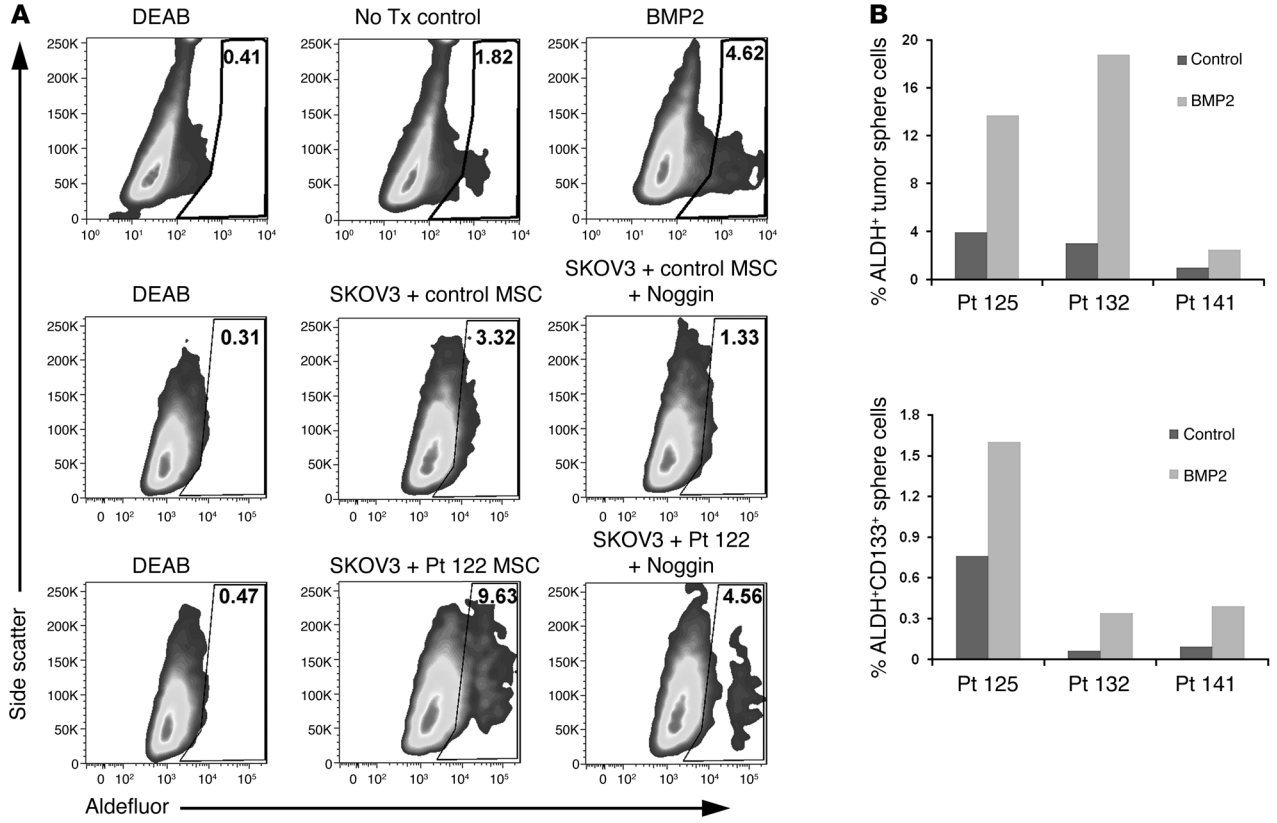

Figure 6

BMP2 increases the percentage of ALDH$^+$ and ALDH$^+$CD133$^+$ CSCs. (**A**) FACS analysis of SKOV3 cells cultured with either PBS (No Tx Control) or BMP2 (100 ng/ml) for 72 hours. FACS analysis of SKOV3 cells cultured in a 1:1 ratio with either adipose control MSCs or CA-MSCs in the absence or presence of Noggin. DEAB control is shown. Numbers represent the percentage of Aldefluor$^+$ cells. (**B**) Results of FACS analysis of primary tumor spheres from 3 different patients treated with PBS (control) or BMP2 (100 ng/ml) for 7 days. The percentage of ALDH$^+$ cells and ALDH$^+$CD133$^+$ cells for each patient sample is shown.

spheroids is an attribute generally associated with CSCs. Quantification of the number of spheres demonstrated a greater than 5-fold increase in spheres in cancer cells cultured with ovarian CA-MSCs compared with that of control MSCs (Figure 4B). FACS analysis of the spheroids demonstrated that tumor spheres were comprised of approximately 80% tumor cells and 20% MSCs (data not shown).

Given the sphere-forming phenotype induced by CA-MSCs, we assayed the cocultured tumor cells for presence of ovarian CSC markers. We and others have recently demonstrated that ALDH is a marker of ovarian CSCs in CD133$^-$ tumor cell lines and primary human tumors (31, 32). We also demonstrated that combined with CD133, ALDH further enhances isolation of ovarian CSC. We therefore analyzed ALDH in DsRED-labeled SKOV3 tumor cells (CD133$^-$ cell line) and ALDH in combination with CD133 in A2780 tumor cells (CD133$^+$ cell line) grown with MSCs. Coculture of SKOV3 cells with control MSCs led to a 2- to 3-fold increase in ALDH$^+$ DsRED SKOV3 cells compared with that of DsRED SKOV3 cells alone, while coculture with CA-MSCs led to an approximate 8-fold increase in the number of ALDH$^+$ carcinoma cells (Figure 4C). Coculture of A2780 cells with control MSCs resulted in a modest (33%) increase in CD133 and no change in the number of ALDH$^+$CD133$^+$ carcinoma cells (Figure 4D). In contrast coculture with CA-MSCs led to a 60% increase in CD133$^+$ cells and an approximate 6-fold increase in CD133$^+$ALDH$^+$ cells (Figure 4D).

Altered ovarian cancer MSC expression patterns. We next attempted to identify genes associated with the functional differences we observed between CA-MSCs and control MSCs. We first used qRT-PCR to analyze the expression of genes previously reported to have altered expression in MSCs associated with cancer, including *IL8*, *GMCSF*, *FGF2*, *CCL5*, and *DKK1* (2, 8, 33). We found that CA-MSCs and MSCs treated with tumor-conditioned media expressed increased levels of both *IL8* and *GMCSF* (Supplemental Figure 4). Interestingly, we observed decreased levels of *CCL5* and *DKK1* and no difference in the expression of FGF2 in CA-MSCs compared with that of controls (Supplemental Figure 4).

In order to identify novel pathways abnormally expressed in CA-MSCs, we used a PCR-based array platform to characterize the expression of MSC-associated genes in CA-MSCs (see Methods for details). We elected to use adipose-derived MSCs as controls, because, unlike BM-MSCs, they demonstrated an enhancement of tumor growth in vivo. In addition, adipose MSCs are likely biologically relevant, as ovarian carcinoma cells often grow in association with omental adipose. As a means to distinguish alterations that may be induced by cancer cell–secreted factors and those that might be unique to ovarian CA-MSCs, we compared the expression pattern of adipose MSCs (n = 3), adipose MSCs treated with tumor-conditioned media (n = 3), and CA-MSCs (n = 3). When the gene expression profile of CA-MSCs was compared with that of

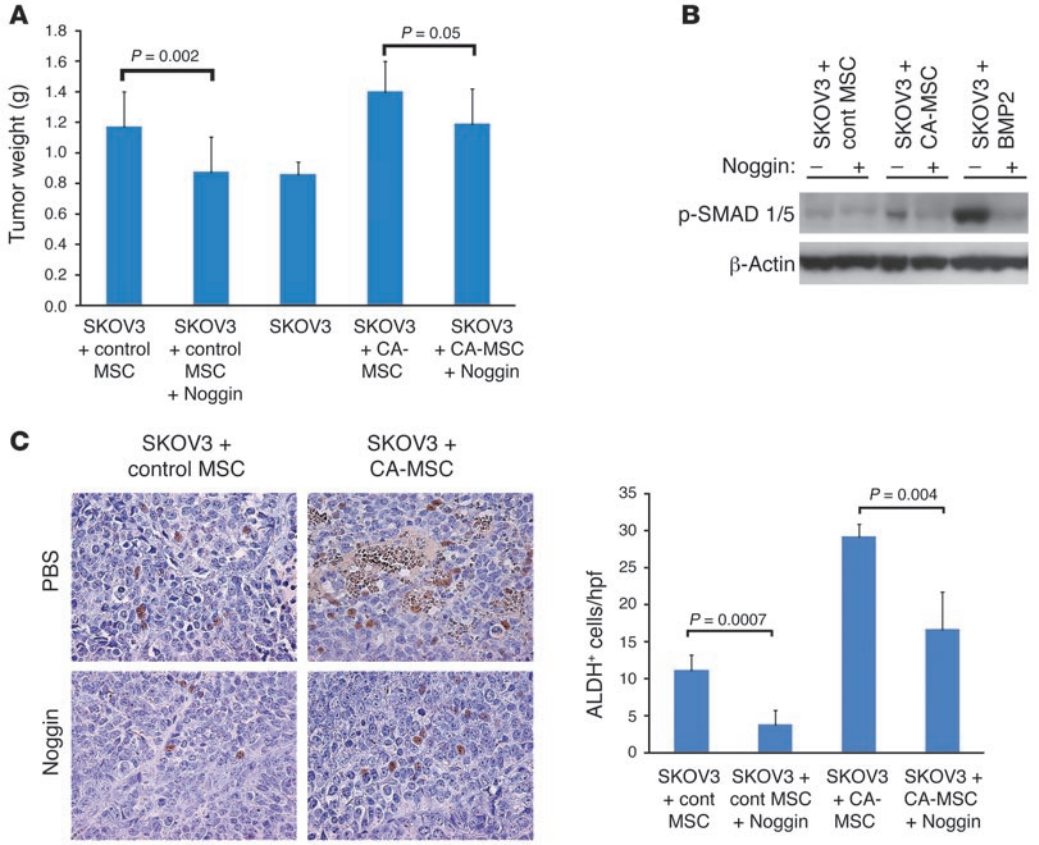

Figure 7

Noggin therapy abrogates MSC-mediated tumorigenesis with an associated decrease in ALDH+ cells. (**A**) At euthanasia, average tumor weights of SKOV3 tumors grown with adipose MSCs (control) or CA-MSCs and treated every 48 hours with Noggin or PBS ($n = 8$ in each group in 2 independent experiments). (**B**) Western blot demonstrating p-SMAD 1/5 and actin controls in the tumors with and without Noggin therapy or BMP2 treatment. (**C**) Representative ALDH1 immunohistochemistry and quantification of ALDH1 expression in the indicated control and Noggin-treated tumors. The number of ALDH+ cells were counted in 10 sections from 4 tumors in each treatment group. Average and standard deviations are indicated with *P* values. Original magnification, ×200. hpf, high-powered field.

control MSCs, we observed 2 sets of genes. One set of genes was differentially expressed in both tumor-conditioned media–treated control MSCs and ovarian CA-MSCs relative to control MSCs (Figure 5A, blue bar). These genes are likely regulated by factors secreted by the tumor cells. However, a second set of genes was differentially expressed solely in the patient-derived MSCs and thus cannot be explained by tumor cell–secreted factors on the cancer MSC phenotype (Figure 5A, orange bar).

Several of the genes upregulated in CA-MSCs are part of the TGF-β superfamily/BMP family, including *BMP2*, *BMP4*, and *BMP6*. We next used qRT-PCR and independent primers in 4 separate CA-MSC lines, control MSCs (including adipose, BM, and normal ovary MSC), and tumor-conditioned media–treated adipose MSCs to confirm the upregulation of *BMP2*, *BMP4*, and *BMP6* mRNAs in CA-MSCs (Figure 5B). Similarly, we confirmed the downregulation of *MMP2*, *PDGFRB*, and *TBX5* (Figure 5B). Furthermore, in order to demonstrate that the changes observed were not an artifact of cell culture, we confirmed increased expression of *BMP2* in CA-MSCs FACS sorted from primary tumors (Figure 5B). Western blot analysis of the BMP2 protein expression level in CA-MSCs versus that in control MSCs confirmed a 3.3-fold increased expression of the BMP2 protein (Figure 5C). These data confirm that CA-MSCs are distinct from control MSCs and implicate the BMP family of proteins as possible mediators of the differential impact of CA-MSCs on tumor growth.

The impact of BMP2 on ovarian tumor cells. Given the altered BMP expression phenotype observed in CA-MSCs, we next explored the role of BMP signaling in ovarian cancer cells. Others have previously reported that BMP2 activates phospho-SMAD signaling in ovarian cancer and is associated with the induction of an epithelial-to-mesenchymal transition (34). Consistent with these reports, we observed that BMP2 treatment of SKOV3 cells in vitro increased levels of phospho-SMAD 1/5 protein, which could be blocked by the BMP2 inhibitor Noggin (Figure 5D). These data indicate BMP2 signaling is active in SKOV3 cells.

To determine whether the ability of CA-MSCs to promote tumor cell stemness was associated with the increased expression of BMP2, we first treated tumor cells with BMP2 in vitro. BMP2 treatment of cancer cells in vitro, analogous to coculture with MSCs, led to an increase in the percentage of ALDH+ tumor cells (Figure 6A). Furthermore, the addition of Noggin to MSC tumor cell cocultures completely blocked control MSC-induced tumor stemness and partially abrogated CA-MSC–associated increases in tumor stemness (Figure 6A). The increase in the percentage of tumor stem cells

was not due to a death of progenitor cells, as we observed tumor cell proliferation and did not observe significant induction of cell death (data not shown). Similar results were also observed with the A2780 ovarian cancer cell line (data not shown).

To confirm these results were not an artifact associated with tumor cell lines, we similarly assayed the impact of BMP2 on primary human ovarian cancer cells using a tumor sphere assay for CSC growth. We used cancer cells from 5 patients with ovarian cancer. Three out of five samples formed spheres. Spheres were treated with BMP2 or mock treated for 1 week and assayed for the percentage of $ALDH^+$ and $ALDH^+CD133^+$ tumor cells. Consistent with our finding in cell lines, primary tumor spheres treated with BMP2 had a 3.2-fold increase in the percentage of $ALDH^+$ tumor cells and a 4.4-fold increase in the percentage of $ALDH^+$ $CD133^+$ tumors cells in BMP2-treated cells versus controls (range, 0.25%–4.0% vs. 4.77%–18% and 0.06%–0.74% vs. 0.33%–1.59% for $ALDH^+$ and $ALDH^+CD133^+$ cells in controls vs. BMP2-treated cells, respectively) (Figure 6B).

Finally, given our observations that BMP inhibition in vitro could reduce tumor stem cell proliferation, we tested the ability of the BMP2 inhibitor Noggin to inhibit MSC-stimulated tumor growth in vivo. Noggin therapy was capable of slowing MSC-stimulated tumor growth of both control MSCs and CA-MSCs (Figure 7A). The tumor-promoting ability of control MSCs could be almost completely abrogated by an excess of Noggin. Human CA-MSC–induced tumorigenesis was partly blocked by Noggin (Figure 7A). Compared with tumors grown with adipose MSCs, tumors grown with CA-MSCs had increased levels of p-SMAD 1/5 proteins (Figure 7B). Similarly, treatment of tumors in vivo with BMP2 was associated with an increase in p-SMAD 1/5 proteins (Figure 7B). Importantly, Noggin treatment of tumors in vivo was associated with a significant decrease in phosphorylated SMAD 1/5 proteins (Figure 7B). Immunohistochemical analysis of the tumors demonstrated that, parallel to that seen in vitro, growth with CA-MSCs was associated with an increase in $ALDH^+$ CSCs, and Noggin treatment was associated with a decrease in the number of $ALDH^+$ cells in both control MSC- and CA-MSC–associated tumors (Figure 7C). FACS analysis confirmed a significant decrease in the number of $ALDH^+$ cells when tumors were treated with Noggin (data not shown).

Taken together, these results strongly suggest that ovarian CA-MSCs promote tumorigenesis via the promotion of ovarian CSC proliferation. Promotion of CSC proliferation is at least in part due to the upregulation of BMP protein expression.

Discussion

To date there has been very little study of human solid tumor-associated MSCs. Our study demonstrates that MSCs are universally present in human ovarian cancer. This is consistent with reports of MSCs present in large numbers of gastric and lung cancers (25, 35). A number of lines of evidence support the statement that the cells we isolated are MSCs and not cancer-associated fibroblasts. First, CA-MSCs demonstrate multipotent differentiation capacity. CA-MSCs could generate adipose, cartilage, and bone in vitro, and our data suggests this may also occur in vivo. In fact, CA-MSC specimens demonstrated greater differentiation capacity than controls. Consistent with this, CA-MSCs demonstrated increased stemness based on an increased expression of ALDH. In addition, unlike fibroblasts, these cells can be stably maintained in culture for more than 6 months, and they continue to maintain multipotent differentiation capacity.

As CA-MSCs do differentiate into fibroblasts, like any MSC samples, a pure MSC culture may not be possible; however, we believe the characteristics we describe of these ovarian cancer-derived cell lines support the conclusion they are at least highly enriched for MSCs. Given the presence of MSCs in solid tumors, it is essential to understand their function and impact on tumorigenesis in vivo. Our data strongly support the tumor-promoting activity of MSCs in the tumor microenvironment. This appears to be at least in part due to MSC secretion of growth factors and the promotion of tumor stem cell proliferation.

The functional phenotype of CA-MSCs. To the best of our knowledge, this study is the first to characterize the function of human solid tumor-associated MSCs in cancer growth. While several early studies indicated that MSCs may inhibit tumor growth (2–4), our study as well as other recent studies find that MSCs significantly enhance tumor growth in immune-deficient mice (8, 10, 36). The reason for the differences in observations among different groups remains unclear. One potential explanation may be different tumor models and microenvironments used to study MSCs. Our studies suggest another potential mechanism — the increase of tumor stemness. Increases in tumor stemness could initially be associated with a reduction in rates of tumor growth, as self-renewal is promoted rather than the production of transient amplifying cells. Later in the course of tumorigenesis, when a critical mass of tumor stem cells is achieved, the CSCs would then undergo differentiation as opposed to self-renewal. With the increased number of stem cells this would then lead to significant expansive tumor growth. Such a biphasic growth pattern maybe particularly evident in slow growing cell lines.

Altered expression in ovarian cancer-associated MSCs. Importantly, we observed that ovarian cancer MSCs are distinct from healthy control MSCs and are more potent at promoting tumor growth. The CA-MSC expression profile may relate in part to the ovarian microenvironment. Normal ovary MSCs appeared to have an expression pattern closer to that of CA-MSCs than did BM-MSCs. Like CA-MSCs, normal ovary MSCs demonstrated a significant downregulation of MMP2, PDGFRβ, and TBX5 relative to that of BM-MSCs and adipose MSCs. Tumor-secreted factors likely play an important role in creating the atypical expression in CA-MSCs. CA-MSCs and adipose MSCs treated with tumor-conditioned media shared a significant overlap in expression profile. This suggests that once in the tumor microenvironment, like other host cells, MSCs are co-opted by the cancer microenvironment to promote tumor growth. Consistent with this, MSCs have been reported to change their expression pattern in the presence of angiogenic growth stimulation (37).

Tumor cell–secreted factors, however, do not explain the entire phenotype of CA-MSCs. CA-MSCs expressed numerous genes that were not seen in control MSCs or control MSCs treated with tumor-conditioned media. The etiology of this upregulation remains unclear. These factors could be induced by other host cells in the tumor microenvironment or require MSC/tumor cell contact. Alternatively, longer treatment with tumor-conditioned media may be necessary to induce these factors. Interestingly, expression of the altered gene expression profile in CA-MSCs is maintained weeks after removal from the tumor microenvironment, suggesting either an autocrine loop is initiated in CA-MSCs or an epigenetic event may take place.

BMP signaling and ovarian cancer. Many of the genes aberrantly regulated in CA-MSCs were BMP family members, with both *BMP2* and *BMP4* showing very significant upregulation in all

CA-MSCs tested. BMP2 and BMP4 often function in a parallel manner and act at the same receptors. BMPs are implicated in both normal developmental tissue homeostasis and tumorigenesis (38). In ovarian cancer, multiple studies have demonstrated that BMP signaling impacts the tumorigenic phenotype. BMP4 signaling has been reported to induce epithelial-mesenchymal transition in vitro in primary human ovarian cancer cells (39). BMP4 has also been reported to drive tumorigenesis of ovarian cancer cells via the regulation of the proto-oncogene ID3 (40). BMP2 has been reported to be specifically upregulated in ovarian cancer cells as compared with normal ovarian surface epithelium (41). BMP2 also appears to have prognostic significance in ovarian cancer patients; BMP2 expression in tumor tissues from ovarian cancer patients has been shown to be inversely correlated with patient survival (34). Finally, the BMP antagonist Chordin was reported to be downregulated in ovarian cancer cells relative to normal ovarian surface epithelium, suggesting overactivation of the BMP pathway could contribute to ovarian tumorigenesis (42).

Our studies contribute to this developing literature supporting a role for BMP proteins in promoting cancer growth. BMPs play an important role in promoting both the primary growth and osteoblastic metastatic disease in prostate cancer. BMP2/4 have also been reported to enhance cell motility and metastases in prostate cancer, gastric cancers, melanoma, and chondrosarcoma (43–46). Similar to results in our studies, Noggin is reported to successfully inhibit prostatic bony metastases (47), to prevent cellular invasion in melanoma, and to decrease metastases in lung cancer (48). While the focus of these studies focused on the impact of MSC factor expression on the tumor cell, MSCs may also respond in an autocrine manner. In response to BMP2/4, MSCs demonstrate increased osteogenic capacity (49). Thus, CA-MSCs and BMP2/4 may promote the formation of microcalcifications commonly observed in ovarian and other tumor types (50, 51).

The impact of MSCs on CSCs. Our studies suggest that ovarian CA-MSCs and BMP signaling play a critical role in the regulation of CSC self-renewal versus differentiation. We observed a 4- to 8-fold increase in the percentage of putative ovarian CSCs in the presence of CA-MSCs both in vitro and in vivo. This was observed with both ovarian tumor cell lines and primary human tumor specimens. Importantly, the effect of CA-MSCs could be replicated with exogenous BMP2 and was in part blocked by the BMP2/4 inhibitor Noggin.

Our work is consistent with recent reports that MSCs can promote the growth of CSCs in vivo (9, 52). While our work establishes a critical role for BMP2 in MSC-associated tumorigenesis, the impact of CA-MSCs on cancer growth and tumor stemness could only partially be blocked by even high doses of the BMP inhibitor Noggin. This suggests that other pathways are also involved in CA-MSC stimulation of tumorigenesis. Consistent with this, a recent report suggests that cancer-associated fibroblasts, which are reported to be derived from MSCs (53), via the secretion of matrix metalloproteinases can induce an epithelial-mesenchymal transition and promote stemness in prostate cancer cells (53).

Origin of CA-MSCs. The exact site of origin of ovarian CA-MSCs remains undetermined. Originally, MSCs were believed to be primarily present in bone marrow or adipose tissue. Numerous studies have indicated that BM-MSCs can home to tumors, thus BM-MSCs could be a source of ovarian CA-MSCs. Given the common association of ovarian tumor cells and omental adipose, CA-MSCs could also be derived from adipose tissue. Interestingly, recent reports suggest that MSCs are present in tissue throughout the body (54). We were able to isolate MSCs from normal ovary, suggesting that tissue resident MSCs could be a source of CA-MSCs.

Two recent reports have suggested that MSC-like cells could be derived directly from CSCs. One study demonstrated that prostate cancer cell lines had the ability to differentiate into osteoblasts and brown adipose. The ability of primary prostate tumor cells to differentiate was not assessed (55). A second study in ovarian cancer suggested that primary $CD133^+$ $EpCAM^+CD44^+$ ovarian CSCs, after passage in mice, could produce mesenchymal cells in vitro (56). This study did not observe mesenchymal differentiation in vivo, and the ability of these cells to differentiate into adipose, bone, or cartilage was not assessed. In contrast, CA-MSCs were clearly $CD133^-EpCAM^-$ and demonstrated an ability to differentiate in multiple tissue types both in vitro and in vivo. Finally, CA-MSCs demonstrated no ability to reverse to an epithelial phenotype, and our epithelial cell clones did not demonstrate an ability to differentiate in vitro (data not shown). Thus we believe that the CA-MSCs we isolated here are distinct from the cells described above. It is possible the CA-MSCs we identified, which expressed CK7, may be related to cancer cells. Further studies will be necessary to confirm that $CK7^+$ CA-MSCs are not nonreversible progeny of ovarian CSCs.

Conclusion. We have identified and characterized MSCs present in human epithelial ovarian cancers. These MSCs have a phenotype that we believe to be unique from that of healthy donor control MSCs. The identification of MSCs in human solid tumors allows for a better understanding of the role of MSCs in human cancer. Our data suggest that the mechanism by which CA-MSCs increase ovarian cancer cell line tumorigenesis in vivo is in part through the BMP signaling pathways that alter the stemness of ovarian tumors. This suggests a potentially new mechanism for CSC regulation and identifies BMP signaling as a potential therapeutic target in ovarian cancer. Continued understanding of the role of MSCs in solid tumors is essential, given that MSCs are being proposed and used in the therapeutic setting.

Methods

Tissue harvesting and culture. Patients consented for tissue donation in accordance with a protocol approved by the University of Michigan's IRB (IRB no. HUM0009149). Fourteen different primary CA-MSC cell lines were generated. CA-MSC lines were isolated from Stage IIIc or Stage IV high-grade papillary-serous or poorly differentiated ovarian (n = 10), fallopian tube (n = 2), or primary peritoneal (n = 2) carcinomas. Tumor samples were obtained from the operating room and immediately taken to the laboratory for processing. Tissue was maintained in RPMI/10% FBS throughout processing. A portion of the tumors were processed to single cell suspensions as previously described (57, 58). Briefly, a portion of each specimen was mechanically dissected and filtered, red cells were lysed with ACK buffer (Lonza Walkersville Inc.), and cells were then washed with media containing serum and plated in MEBM (Lonza) supplemented with 10% heat-inactivated FBS, 1X B27, 20 ng/ml EGF, 1 ng/ml hydrocortisone, 5 μg/ml insulin, 100 μM β-mercaptoethanol, 10 ng/ml β-FGF, 1% penicillin/streptomycin, and 20 μg/ml gentamicin. Alternatively, a fresh 4 × 4 × 2–mm tumor slice was rinsed several times to remove all loosely attached cells. The tissue was then placed in a tissue culture dish in a thin layer of MEBM and covered with a sterile cover glass to increase tissue contact with the dish. After 24 hours, the tissue was removed, and adherent cells were washed aggressively and cultured in MEBM. When CFU-F were apparent from either culture method, the cells were trypsinized and

replated in limiting dilutions in MEBM. Individually arising CFU-F were then isolated and expanded in traditional mesenchymal media. Phenotypes of CFU-F from the 2 approaches were similar.

In order to isolate epithelial cells, whole tumor cell suspensions were plated in MesenCult MSC Basal Medium for Human Mesenchymal Stem Cells with Mesenchymal Stem Cell Stimulatory Supplements (StemCell Technologies). Under these conditions, tumor cells soon dominated the culture. Cells were then trypsinized and replated in limiting dilutions, and then individual epithelial clones were easily identified and isolated.

Ovarian cancer cell lines SKOV3, A2780, and Hey1 were obtained from ATCC and cultured in RPMI with 10% FBS (Invitrogen). As MSC-positive controls, normal healthy donor, adipose-derived MSCs were obtained (Invitrogen). BM-MSCs were provided by Max Wicha (University of Michigan).

Flow cytometry. The following antibodies were used for flow cytometric analysis of putative MSCs: anti-CD133/2-APC (Miltenyi Biotec); anti–CD44-PE and anti–CD44-FITC (BD Pharmingen); anti–hCD90-APC and anti–hCD90-PE (R&D Systems); anti–CD105-FITC and anti–CD105-APC (Abcam); anti–CD45-FITC, anti–CD45-APC, and anti–CD45-PE (BD Pharmingen); anti-CD34 (BD Pharmingen); anti-SH3 (BD Pharmingen); and anti-CD144 (VE-cadherin)-PE (eBioscience). The Aldefluor assay was performed as per the manufacturer's instructions (StemCell Technologies). Flow cytometric analysis was performed on a BD Biosciences FACSCalibur through the University of Michigan Flow Cytometry Core, and data analysis was performed using FlowJo (Tree Star Inc.).

Differentiation assays. For bone differentiation, cells were plated at 5×10^4 cells/well of a 6-well plate in either StemPro Osteogenesis Differentiation Media (Invitrogen) or control media and then allowed to grow for approximately 14 days, with media changed twice per week. Cells were then rinsed with PBS, fixed with 3.7% formaldehyde, rinsed with water, stained with 2% Alizarin Red S (Sigma-Aldrich) solution (pH 4.2) for 2 minutes, and washed with distilled water. For cartilage differentiation, cells were plated in 5- to 10-μl micromass droplets onto a dry plate from a solution of 1.6×10^7 cells/ml, allowed to set for 2 hours, and then incubated in either StemPro Chondrogenesis Differentiation Media (Invitrogen) or control media. Cells were allowed to grow for approximately 14 days with media changed twice per week and then rinsed with PBS, fixed with 4% formaldehyde, rinsed with PBS, stained for 30 minutes with 1% Alcian Blue solution (Sigma-Aldrich) prepared in 0.1 N HCl, and washed with 0.1 N HCl. For adipose differentiation, cells were plated at 5×10^4 cells/well of a 6-well plate, in either differentiation media (StemCell Technologies) or control media, and the media was changed weekly. After 14 to 21 days, cells were fixed with 3.7% formaldehyde, stained with 0.3% Oil Red O (Fisher Scientific) for 1 hour, and washed with water.

Karyotyping. CA-MSCs were cultured under conditions as described above, and then once they had reached 60%–70% confluence in the log phase of growth, they were fixed in buffer provided by Cell Line Genetics, to whom cells were then provided for commercial karyotyping using colcemid.

Isolation of single cell clones. Cells were trypsinized and then resuspended in limiting dilutions of MesenCult media (~1 cell/50 μl, StemCell Technologies). Cells were then plated in 96-well dishes, and single cells were confirmed by microscopy. Clones were allowed to grow until they were confluent and were then trypsinized, passaged to a 24-well plate, allowed to grow to confluence, and passaged a second time. Only the colonies that successfully passaged twice were deemed true clones.

Coculture experiment. SKOV3-dsRed or A2780-dsRED tumor cells were plated with MSCs at 1:1 with a mixed medium (50:50, RPMI/MEBM), grown for 24 hours, and then treated with Noggin at 200 ng/ml or mock treated. Cultures were then observed daily under light microscopy. Cells were trypsinized and resuspended in PBS for FACS analysis performed with the antibodies and method as described above. Alternatively, spheres present in the supernatant were collected by 3 rounds of gentle washing, trypsinized, and then analyzed by FACS as above.

PCR array and RT-PCR. MSCs were cultured with complete medium to 80% confluence and washed once with ice-cold PBS, before being homogenized in 3 ml TRizol reagent (Invitrogen). Total RNA was extracted with the PureLink Total RNA Purification System (Invitrogen) with on-column DNase treatment. RNA quality was examined on a Bioanalyzer 2100 (Agilent). We used a human MSC PCR array (SABiosciences), containing 84 target genes involved in MSC pluripotency, differentiation, and self-renewal. For the PCR array, first-strand cDNA was synthesized with the SABiosciences RT² First Strand Kit; for all other real-time PCR experiments, first-strand cDNA was synthesized with the SuperScript III First-Strand Synthesis System for RT-PCR (Invitrogen) according to the manufacturer's recommendations. Two μg total RNA was used for each reaction. SYBR green–based array PCR was performed using the 7900 HT Sequence Detection System (Applied Biosystems); the other real-time PCR was performed using the StepOne System (Applied Biosystems) and the indicated primer (Supplemental Table 1). The comparative Ct method was used for data analysis described at RT² Profiler PCR Array Data Analysis (SABiosciences; http://www.sabiosciences.com/pcr/arrayanalysis.php).

Immunoblotting. To detect BMP2 protein expression in MSCs, cells were grown in 60-mm dishes to 80% confluence. Protein transport inhibitor GolgiPlug (BD Science) was added at 1 μl/ml for 4 hours. To detect phospho-SMAD 1/5 after BMP2 (R&D Systems) treatment, MSCs were grown in 60-mm dishes to 60% confluence with complete medium and then serum starved for 16 hours. BMP stimulation was carried out at 200 ng/ml for 30 minutes. SKOV3 cells were also stimulated with or without 50% MSC-conditioned medium for 30 minutes. Cells were washed 2 times with ice-cold PBS before lysis in 200 μl RIPA buffer (Invitrogen) with complete proteinase inhibitor and phosphatase inhibitor (Roche). Insoluble material was removed by centrifugation at 16,000 *g* at 4°C for 15 minutes. Protein concentrations were determined using the Bradford Protein Assay Kit (Bio-Rad). Lysates containing 10 μg total protein were separated on 4%–12% NuPAGE SDS gel (Invitrogen) and transferred onto a nitrocellulose membrane. Antibodies used for Western blot analysis include anti-BMP2 (1:800 dilution, Abcam), anti–p-SMAD 1/5 and anti-SMAD 5 (1:1,000 dilution, Cell Signaling Technology), and anti–β-actin (1:10,000 dilution, Sigma-Aldrich). Bands were visualized using the ECL Kit (Pierce, Thermo Scientific).

In vitro MSC-conditioned medium. 1×10^6 control MSCs or CA-MSCs were plated in 10-cm dishes with MEBM supplemented with 10% FBS as mentioned above, grown to 50% confluence, and then switched to a plain MEBM plus 5% charcoal-stripped FBS. After 2 days, the MSC medium was harvested, filtered (0.2-μm filter), mixed with RPMI 1640 supplemented with 10% FBS (1:1, v/v), and then plated at 40% confluence with the ovarian cancer tumor cells SKOV3, Hey1, or A2780 for 3 days. Tumor cells were washed, trypsinized, and resuspended in PBS for FACS analysis or lysed in TRIzol reagent for total RNA extraction.

In vitro tumor-conditioned medium. 5×10^5 SKOV3 or Hey1 cells were plated in 10-cm dishes, grown to 40% confluence in RPMI 1640 supplemented with 10% FBS, and then switched to RPMI 1640 containing 5% charcoal-stripped FBS. Two days later, the tumor medium was collected, filtered on a 0.2-μm filter, mixed with 50% complete MEBM growth medium, and then plated at 40% confluence of the MSCs for 3 days. MSCs were washed and lysed in TRIzol reagent for total RNA extraction.

Human tumor sphere assay. 1×10^6 freshly isolated human ovarian tumor cells were plated in ultralow-adherence plates in MEBM supplemented with 20 ng/ml EGF, 5 μg/ml insulin, and 10 ng/ml β-FGF. After 24 hours, cells replicates were treated with 100 ng Noggin (R&D Systems). After

72 hours, fresh media with or without Noggin was added, and then after an additional 72 hours, spheres were mechanically separated using a syringe and ultralow-dose trypsin (0.05%) and analyzed via flow cytometry as described above.

Animal studies. NOD/SCID mice were obtained from Charles River Laboratories. Animals were maintained in accordance with institutional policies, and all studies were performed with approval of the University Committee on Use and Care of Animals of the University of Michigan. To generate tumors, 1×10^6 tumor cells were injected in 300 μl of growth factor–reduced Matrigel (BD Biosciences) into the axillae of immunodeficient mice. 5×10^5 tumor cells with 5×10^5 MSCs were injected with Matrigel in the contralateral axilla. All studies were done using early-passage ovarian cancer MSCs (passage 3–8). Tumor growth was measured using calipers, and volumes were calculated based on the modified ellipsoid formula ($L \times W \times W/2$), where L represents length, and W represents width.

Tumor imaging. SKOV3 tumor cells were stably transduced with a luciferase-expressing lentivirus (plentiloxEV-Luc virus, provided by the vector core at the University of Michigan). The coinjection experiments were carried out with 1×10^6 SKOV3-Luc cells alone (n = 10) or a 1:1 mixture of control MSCs (n = 10) or CA-MSCs (n = 10). Bioluminescence optical imaging (Xenogen IVIS 2000, Caliper Life Sciences) was first obtained 7 days after tumor cell injection and then measured every other day thereafter for 10 days. Ten minutes prior to imaging, each mouse was given an i.p. injection with 100 μl coelenterazine in PBS at 40 mg/ml. During the imaging, general anesthesia was given with 2% isoflurane (IsoSol, Medeva Pharmaceuticals Inc.). Luminescence images were acquired for 3 seconds to 1 minute. The optical signal was expressed as radiance in units of photons/second/centimeter^2 (p/s/cm^2).

Noggin therapy. For the in vivo Noggin experiments, cells were pretreated with or without Noggin (R&D Systems) at 200 ng/ml for 60 minutes and injected into contralateral axillae with 200 ng Noggin. Mice were treated with PBS or Noggin (200 ng) subcutaneously every 48 hours for 5 doses. Mice were imaged as above starting at day 7 and every 48–72 hours until sacrifice. For Western blot analysis, a subset of tumors were treated with Noggin daily for 48 hours prior to harvesting tumors. Tumors were collected 4 hours after the final treatment, and a portion of each tumor was snap frozen and then lysed in RIPA buffer with phosphatase inhibitors and protease inhibitors.

Immunohistochemistry. A portion of each tumor was fixed in 10% formalin for 2 hours at room temperature and then transferred to 70% ethanol. Tumors were then paraffin embedded and stained at the histology core at the University of Michigan using EDTA-based antigen retrieval and mouse anti-ALDH antibody (BD Biosciences, clone 44/ALDH; 1:100) or anti-Ki67 antibody (Abcam no. 15580, 1:2,000). For stain quantification, 8–10 sections from 4 to 5 tumors per treatment group were analyzed. For ALDH, cells were counted from 10 high-power fields per section (×400). For Ki67, cells were counted from 4 low-power fields (×100) per section. Counts were then compared using a 2-sided Student's t test.

Statistics. P values of less than 0.05 were considered statistically significant.

Acknowledgments

This work was generously supported by the Clinical Investigator Award of the Damon Runyon Cancer Research Foundation. Evan Keller and Laurie McCauley were supported by National Cancer Institute grant P01 093900. We would like to thank Max Wicha for constructive discussions throughout the course of this work and Kornelia Polyak for her reading and review of the manuscript. We are indebted to the Flow Cytometry core at the University of Michigan.

Received for publication September 30, 2010, and accepted in revised form May 11, 2011.

Address correspondence to: Ronald J. Buckanovich, Rm 5219 Cancer Center, 1500 E. Medical Center Drive, Ann Arbor, Michigan 48109, USA. Phone: 734.764.2395; Fax: 734.936.7376; E-mail: ronaldbu@med.umich.edu.

1. Stagg J. Mesenchymal stem cells in cancer. *Stem Cell Reviews*. 2008;4(2):119–124.
2. Qiao L, Xu Z-L, Zhao T-J, Ye L-H, Zhang X-D. Dkk-1 secreted by mesenchymal stem cells inhibits growth of breast cancer cells via depression of Wnt signalling. *Cancer Letters*. 2008;269(1):67–77.
3. Zhu Y, et al. Human mesenchymal stem cells inhibit cancer cell proliferation by secreting DKK-1. *Leukemia*. 2009;23(5):925–933.
4. Lu Y-R, et al. The growth inhibitory effect of mesenchymal stem cells on tumor cells in vitro and in vivo. *Cancer Biol Ther*. 2008;7(2):245–251.
5. Ramasamy R, Lam EWF, Soeiro I, Tisato V, Bonnet D, Dazzi F. Mesenchymal stem cells inhibit proliferation and apoptosis of tumor cells: impact on in vivo tumor growth. *Leukemia*. 2007;21(2):304–310.
6. Djouad F, et al. Immunosuppressive effect of mesenchymal stem cells favors tumor growth in allogeneic animals. *Blood*. 2003;102(10):3837–3844.
7. Muehlberg FL, et al. Tissue-resident stem cells promote breast cancer growth and metastasis. *Carcinogenesis*. 2009;30(4):589–597.
8. Karnoub AE, et al. Mesenchymal stem cells within tumour stroma promote breast cancer metastasis. *Nature*. 2007;449(7162):557–563.
9. Liu S, et al. Breast cancer stem cells are regulated by mesenchymal stem cells through cytokine networks. *Cancer Res*. 2011;71(2):614–624.
10. Spaeth EL, et al. Mesenchymal stem cell transition to tumor-associated fibroblasts contributes to fibrovascular network expansion and tumor progression. *PLoS One*. 2009;4(4):e4992.
11. Buckanovich RJ, et al. Tumor Vascular Proteins as Biomarkers in Ovarian Cancer. *J Clin Oncol*. 2007;25(7):852–861.
12. St Croix B, et al. Genes expressed in human tumor endothelium. *Science*. 2000;289(5482):1197–1202.
13. Haviv I, Polyak K, Qiu W, Hu M, Campbell I. Origin of carcinoma associated fibroblasts. *Cell Cycle*. 2009;8(4):589–595.
14. Mantovani A, Schioppa T, Porta C, Allavena P, Sica A. Role of tumor-associated macrophages in tumor progression and invasion. *Cancer Metastasis Rev*. 2006;25(3):315–322.
15. Arnulf B, et al. Phenotypic and functional characterization of bone marrow mesenchymal stem cells derived from patients with multiple myeloma. *Leukemia*. 2007;21(1):158–163.
16. Jootar S, et al. Bone marrow derived mesenchymal stem cells from chronic myeloid leukemia t(9;22) patients are devoid of Philadelphia chromosome and support cord blood stem cell expansion. *Leuk Res*. 2006;30(12):1493–1498.
17. Zhao Z-G, et al. Phenotypic and functional comparison of mesenchymal stem cells derived from the bone marrow of normal adults and patients with hematologic malignant diseases. *Stem Cells Dev*. 2007;16(4):637–648.
18. Garayoa M, et al. Mesenchymal stem cells from multiple myeloma patients display distinct genomic profile as compared with those from normal donors. *Leukemia*. 2009;23(8):1515–1527.
19. Gibbs CP, et al. Stem-like cells in bone sarcomas: implications for tumorigenesis. *Neoplasia*. 2005;7(11):967–976.
20. Lin TM, et al. Isolation and identification of mesenchymal stem cells from human lipoma tissue. *Biochem Biophys Res Commun*. 2007;361(4):883–889.
21. Yu Y, et al. Mesenchymal stem cells and adipogenesis in hemangioma involution. *Stem Cells*. 2006;24(6):1605–1612.
22. Matushansky I, et al. Derivation of sarcomas from mesenchymal stem cells via inactivation of the Wnt pathway. *J Clin Invest*. 2007;117(11):3248–3257.
23. Tasso R, et al. Development of sarcomas in mice implanted with mesenchymal stem cells seeded onto bioscaffolds. *Carcinogenesis*. 2009;30(1):150–157.
24. Chiba H, et al. CD105-positive cells in pulmonary arterial blood of adult human lung cancer patients include mesenchymal progenitors. *Stem Cells*. 2008;26(10):2523–2530.
25. Cao H, et al. Mesenchymal stem cell-like cells derived from human gastric cancer tissues. *Cancer Lett*. 2009;274(1):61–71.
26. Pittenger MF, et al. Multilineage potential of adult human mesenchymal stem cells. *Science*. 1999;284(5411):143–147.
27. Chamberlain G, Fox J, Ashton B, Middleton J. Concise review: mesenchymal stem cells: their phenotype, differentiation capacity, immunological features, and potential for homing. *Stem Cells*. 2007;25(11):2739–2749.
28. Beckermann BM, et al. VEGF expression by mesenchymal stem cells contributes to angiogenesis in pancreatic carcinoma. *Br J Cancer*. 2008;99(4):622–631.
29. Galie M, et al. Mesenchymal stem cells share molecular signature with mesenchymal tumor cells and favor early tumor growth in syngeneic mice. *Oncogene*. 2008;27(18):2542–2551.
30. Qiao L, et al. Suppression of tumorigenesis by human mesenchymal stem cells in a hepatoma

model. *Cell Res*. 2008;18(4):500–507.
31. Deng S, et al. Distinct expression levels and patterns of stem cell marker, aldehyde dehydrogenase isoform 1 (ALDH1), in human epithelial cancers. *PLoS One*. 2010;5(4):e10277.
32. Silva IA, et al. Characterization of ovarian CSC using ALDH and CD133 identifies a cancer stem cell hierarchy. AACR Meeting Abstracts. 2010:403.
33. Hofer EL, et al. Mesenchymal stromal cells, colony-forming unit fibroblasts, from bone marrow of untreated advanced breast and lung cancer patients suppress fibroblast colony formation from healthy marrow. *Stem Cells Dev*. 2010;19(3):359–370.
34. Le Page C, et al. BMP-2 signaling in ovarian cancer and its association with poor prognosis. *J Ovarian Res*. 2009;2:4.
35. Chiba H, et al. CD105-positive cells in pulmonary arterial blood of adult human lung cancer patients include mesenchymal progenitors. *Stem Cells*. 2008;26(10):2523–2530.
36. Zhu W, et al. Mesenchymal stem cells derived from bone marrow favor tumor cell growth in vivo. *Exp Mol Pathol*. 2006;80(3):267–274.
37. Campioni D, Lanza F, Moretti S, Ferrari L, Cuneo A. Loss of Thy-1 (CD90) antigen expression on mesenchymal stromal cells from hematologic malignancies is induced by in vitro angiogenic stimuli and is associated with peculiar functional and phenotypic characteristics. *Cytotherapy*. 2008;10(1):69–82.
38. Waite KA, Eng C. From developmental disorder to heritable cancer: it's all in the BMP/TGF-beta family. *Nat Rev Genet*. 2003;4(10):763–773.
39. Theriault BL, Shepherd TG, Mujoomdar ML, Nachtigal MW. BMP4 induces EMT and Rho GTPase activation in human ovarian cancer cells. *Carcinogenesis*. 2007;28(6):1153–1162.
40. Shepherd TG, Theriault BL, Nachtigal MW. Autocrine BMP4 signalling regulates ID3 proto-oncogene expression in human ovarian cancer cells. *Gene*. 2008;414(1–2):95–105.
41. Le Page C, et al. Gene expression profiling of primary cultures of ovarian epithelial cells identifies novel molecular classifiers of ovarian cancer. *Br J Cancer*. 2006;94(3):436–445.
42. Moll F, et al. Chordin is underexpressed in ovarian tumors and reduces tumor cell motility. *FASEB J*. 2006;20(2):240–250.
43. Ye L, Lewis-Russell JM, Kyanaston HG, Jiang WG. Bone morphogenetic proteins and their receptor signaling in prostate cancer. *Histol Histopathol*. 2007;22(10):1129–1147.
44. Fong YC, et al. BMP-2 increases migration of human chondrosarcoma cells via PI3K/Akt pathway. *J Cell Physiol*. 2008;217(3):846–855.
45. Rothhammer T, Poser I, Soncin F, Bataille F, Moser M, Bosserhoff AK. Bone morphogenic proteins are overexpressed in malignant melanoma and promote cell invasion and migration. *Cancer Res*. 2005;65(2):448–456.
46. Kang MH, Kim JS, Seo JE, Oh SC, Yoo YA. BMP2 accelerates the motility and invasiveness of gastric cancer cells via activation of the phosphatidylinositol 3-kinase (PI3K)/Akt pathway. *Exp Cell Res*. 2010;316(1):24–37.
47. Feeley BT, et al. Overexpression of noggin inhibits BMP-mediated growth of osteolytic prostate cancer lesions. *Bone*. 2006;38(2):154–166.
48. Feeley BT, et al. Mixed metastatic lung cancer lesions in bone are inhibited by noggin overexpression and Rank:Fc administration. *J Bone Miner Res*. 2006;21(10):1571–1580.
49. Kang Q, et al. A comprehensive analysis of the dual roles of BMPs in regulating adipogenic and osteogenic differentiation of mesenchymal progenitor cells. *Stem Cells Dev*. 2009;18(4):545–559.
50. Burkill GJ, Allen SD, A'Hern R P, Gore ME, King DM. Significance of tumour calcification in ovarian carcinoma. *Br J Radiol*. 2009;82(980):640–644.
51. Okada S, et al. Calcifications in mucinous and serous cystic ovarian tumors. *J Nippon Med Sch*. 2005;72(1):29–33.
52. Quintana E, Shackleton M, Sabel MS, Fullen DR, Johnson TM, Morrison SJ. Efficient tumour formation by single human melanoma cells. *Nature*. 2008;456(7222):593–598.
53. Giannoni E, et al. Reciprocal activation of prostate cancer cells and cancer-associated fibroblasts stimulates epithelial-mesenchymal transition and cancer stemness. *Cancer Res*. 2010;70(17):6945–6956.
54. Crisan M, et al. A perivascular origin for mesenchymal stem cells in multiple human organs. *Cell Stem Cell*. 2008;3(3):301–313.
55. Zhau HE, et al. Human prostate cancer harbors the stem cell properties of bone marrow mesenchymal stem cells. *Clin Cancer Res*. 2011;17(8):2159–2169.
56. Strauss R, et al. Analysis of epithelial and mesenchymal markers in ovarian cancer reveals phenotypic heterogeneity and plasticity. *PLoS One*. 2011;6(1):e16186.
57. Conejo-Garcia JR, et al. Vascular leukocytes contribute to tumor vascularization. *Blood*. 2005;105(2):679–681.
58. Pulaski HL, et al. Identifying alemtuzumab as an anti-myeloid cell antiangiogenic therapy for the treatment of ovarian cancer. *J Transl Med*. 2009;7:49.